Applied Catalysis B: Environmental 156–157 (2014) 202–212

Contents lists available at ScienceDirect

Applied Catalysis B: Environmental

journal homepage: www.elsevier.com/locate/apcatb

Insights into dynamic surface processes occurring in Rh supported on Zr-grafted γ-Al_2O_3 during dry reforming of methane

Camila Fernández[a,*], Nicole Miranda[a], Ximena García[a], Pierre Eloy[b], Patricio Ruiz[a], Alfredo Gordon[a], Romel Jiménez[a]

[a] Departamento de Ingeniería Química, Universidad de Concepción, Concepción, Chile
[b] Institute of Condensed Matter and Nanosciences (IMCN), Molecules, Solids and Reactivity (MOST) Division, Université Catholique de Louvain, Croix du Sud 2/17, 1348 Louvain-la-Neuve, Belgium

ARTICLE INFO

Article history:
Received 25 September 2013
Received in revised form 8 March 2014
Accepted 11 March 2014
Available online 20 March 2014

Keywords:
Dry methane reforming
Rh on Zr-grafted alumina catalyst
Mechanical mixtures
Synergistic effect
Oxygen species mobility

ABSTRACT

γ-Al_2O_3 support was modified with zirconia by the grafting method, using zirconium(IV) n-propoxide as precursor. Rh catalysts were prepared by wet impregnation of pure γ-Al_2O_3 (Rh/A), Zr modified γ-Al_2O_3 (Rh/100Z-A), and pure ZrO_2 (Rh/Z) supports. Rh/A presents a good activity in dry reforming of methane and exhibits a high amount of surface oxidized rhodium (92% of surface Rh atoms) after the reaction. Rh/Z is poorly active and 45% of Rh surface atoms remain reduced during the reaction. The catalytic activity significantly increased when using Rh/100Z-A. Tetragonal ZrO_2 crystallites are formed on the surface of modified alumina. It was obtained that, after Rh deposition, the grafted catalyst is composed by Rh/A and Rh/Z, as separated catalytic particles in good contact. To further understand the high activity of the grafted catalyst, mechanical mixtures of Rh/A and Rh/Z catalysts were synthesized. Compared with the single catalysts, an important synergistic effect in methane conversion and yields to CO and H_2 was observed when high amounts of Rh/A were mixed with Rh/Z catalyst, along with a promotion of rhodium oxidation in Rh/Z, which leads to a high surface fraction of RhO_x (88%) in the mixture. The formation of mixed phases between the supports and the migration of Rh atoms from one phase to the other were discarded. It is suggested that a catalytic cooperation occurs due to the presence and mobility of oxygen species generated by the dissociation of CO_2 on Rh/A, which migrate to the Rh/Z catalyst promoting the oxidation of rhodium at its surface, and the catalytic activity. This cooperation mechanism is also expected to operate in the Rh/100Z-A catalyst, between the Rh/A and Rh/Z particles present in the surface. The importance of oxidized Rh for dry reforming of methane is evident from the high catalytic activity achieved when highly oxidized rhodium atoms are present together with the metallic Rh sites where methane activation occurs.

1. Introduction

Dry reforming of methane (DRM) to synthesis gas is an interesting way to utilize and abate two important greenhouse gases (CO_2 and CH_4). Synthesis gas is a valuable feedstock both, for the production of higher hydrocarbons (Fischer–Tropsch synthesis) and for carbonylation processes [1,2]. It has been shown that the kinetically relevant step is the C—H bond activation on the catalyst surface [3,4], a structure-sensitive reaction favored in stepped and kinked surfaces [3], which may lead to a high carbon formation [5] and thus, to the fast deactivation of the catalyst.

Rh/γ-Al_2O_3 catalysts exhibit a high activity and stability in the DRM reaction, being the metallic Rh atoms reported as the active sites [6–17]. However, high temperature oxidation treatments lead to severe catalyst deactivation, due to the strong interaction between rhodium oxides and alumina, which drastically decreases the reducibility of rhodium [18]. It has been suggested that the introduction of ZrO_2 decreases metal–alumina interactions [19], by avoiding the formation of metal aluminate (MAl_2O_4) spinel species reported for many alumina-supported metal samples (e.g. Rh, Pt and Ni) [18,20]. Furthermore, ZrO_2 addition has been shown to be a key factor of coking prevention in the DRM process, thus allowing a higher stability of the catalysts [20–22].

* Corresponding author. Present address: Institute of Condensed Matter and Nanosciences (IMCN), Molecules, Solids and Reactivity (MOST) Division, Université Catholique de Louvain, Croix du Sud 2/17, 1348 Louvain-la-Neuve, Belgium.
Tel.: +32 010 47 36 60.
E-mail addresses: camila.fernandez@uclouvain.be, fernandez.r.ca@gmail.com (C. Fernández).

http://dx.doi.org/10.1016/j.apcatb.2014.03.023
0926-3373/

The aim of this work is to provide a new insight into the role of zirconium oxide in the catalytic performance for DRM. The results presented here may be useful to supplement and explain previous results. They will show that oxidized rhodium atoms may promote the activation of methane over metallic Rh sites, and that the presence of Zr favors the oxidation of rhodium under reaction conditions, then improving the activity and stability of the catalyst.

An advantageous method to modify the surface of a support is the grafting technique, which allows the bonding of small amounts of a metal complex precursor to the hydroxyls of the support, and the subsequent in situ formation of oxides structures from such complexes. This method leads to a great number of high quality contacts between the support and the metal oxides incorporated on its surface with a high dispersion, a high resistance to sintering and good mechanical properties [23–25].

In the first part of this work, the grafting method was used to incorporate ZrO_2 on the surface of the γ-Al_2O_3 support, before the impregnation of Rh, providing the conditions for a high number of contact points between ZrO_2 and γ-Al_2O_3. It is expected that rhodium atoms be deposited on the ZrO_2 crystallites formed by grafting and/or over the remaining non-modified alumina surface, and thus be the catalyst comprising Rh/γ-Al_2O_3 and Rh/ZrO_2 phases. We show that a higher activity is obtained for this modified catalyst.

To clarify the role of the ZrO_2 in the improvement of catalytic performance, in the second part of the work, the contact existing between Rh/γ-Al_2O_3 and Rh/ZrO_2 particles forming part of the modified catalyst was experimentally simulated by gently mixing Rh/γ-Al_2O_3 and Rh/ZrO_2 single catalysts (separately prepared). The aim of preparing mechanical mixtures is to put both catalytic phases in contact with a minimal interaction, thereby avoiding any chemical contamination or formation of new oxide phases, that could difficult the interpretation of results. We show ahead that mechanical mixtures give important insights to explain the catalytic activity of the Rh catalyst supported on Zr modified alumina.

2. Experimental

2.1. Synthesis of catalysts

2.1.1. Grafted alumina

Modified alumina support, denoted as 100Z-A, was prepared by the organic grafting technique. The γ-Al_2O_3 support (10 g, Alfa Aesar, SBET = 72 m^2/g) was added to a solution containing Zirconium(IV) n-propoxide (Merck, >98%) in n-propanol (50 ml, Merck, 99.8%). The amount of Zr precursor is that required to form a ZrO_2 theoretical monolayer on the alumina surface (corresponding to 9.6 wt.% of ZrO_2 in the support), which considers a conventional stoichiometry of one ZrO_2 molecule to one hydroxyl group, and that the ZrO_2 molecule has a circular projection with a radius equal to 0.226 nm [26]. After 2 h of stirring the solution at room temperature, the solvent was removed under reduced pressure in a rotavapor at 30 °C. The recovered solid was dried at 110 °C overnight, before its calcination in air at 500 °C during 5 h.

2.1.2. Rh-supported catalysts

The Rh catalysts were prepared by wet impregnation of pure alumina (Rh/A), Zr modified alumina (Rh/100Z-A), and pure zirconia (Rh/Z) supports (Alfa Aesar, SBET = 4 m^2/g). In each case, 5 g of the powdered support were dipped into deionized water and 180 mg of ammonium hexachlororhodate (Alfa Aesar, 28 wt.% of Rh) were added to the solution to obtain a theoretically 1 wt.% of Rh catalyst. After stirring for two hours at room temperature, the solvent was evaporated in a rotavapor at 35 °C under reduced pressure. The resulting solid was dried overnight at 110 °C and later calcined in air for 4 h at 700 °C.

2.1.3. Mechanical mixtures

Mixtures of Rh/A and Rh/Z, in different percentages (25, 50 and 75 wt.%), were obtained by dispersing both catalysts in n-pentane (Merck, >98%) under vigorous agitation assisted by ultrasonic dispersion. The n-pentane was evaporated under agitation at 25 °C and the recovered solid was dried overnight at 110 °C. After drying, the mixtures were not calcined. The single Rh/A and Rh/Z catalysts were subjected to exactly the same treatment as the mixtures. Samples are denoted as Rh/A, 75Rh/A + 25Rh/Z, 50Rh/A + 50Rh/Z, 25Rh/A + 75Rh/Z and Rh/Z, the number indicating the weight percentage of each catalytic component (Rh/A and Rh/Z).

Samples denoted as 'fresh' correspond to calcined catalysts, while samples denoted as 'tested' correspond to catalysts obtained after the catalytic test, which includes the reduction pretreatment and the subsequent reaction.

2.2. Catalytic activity measurements

2.2.1. Catalytic tests

30 mg of catalyst was tested under atmospheric pressure in a fixed-bed quartz reactor (i.d. 4.5 mm). The catalyst was diluted with quartz sand (quartz/catalyst ratio = 3), to reduce radial and axial temperature gradients in the bed and suppress effects such as axial dispersion and bypassing. The catalyst and inert particles were previously sieved to obtain the particle size range selected according to mass transfer limitations criteria discussed in Section 2.2.2. The catalytic bed was held by quartz wool and the temperature was monitored using a K-type thermocouple located immediately above the quartz wool bed. Another K-type thermocouple was used to measure and control the temperature nearby the external reactor wall. In all experiments, both temperatures were similar.

Before performing the reaction, the catalyst was reduced in situ by increasing the temperature (10 °C/min) from room temperature to 700 °C in pure H_2 (Indura SA, >99.99%) flow (80 ml/min), and soaking the sample at 700 °C for 1 h. Then, the system was flushed with helium during 15 min.

The reaction was carried out in a flowing mixture (300 ml/min) of CH_4/CO_2/He (5/5/90 vol.%), all the gases provided by Indura SA with purity >99.99%. A high dilution in helium allows to manage the rate of heat production, avoiding cold spots that could promote undesirable reactions such as the reverse Boudouard reaction ($2CO \rightarrow C + CO_2$).

Isothermal (600 °C) and non-isothermal (450–700 °C) experiments were performed; space velocities (6×10^5 ml/h/g_{cat} and 1.63×10^5 ml/h/g_{cat}) were such that conversions were far from thermodynamic equilibrium. Indeed, the parameter that has been reported as a measure of the approach to equilibrium ($r = r_{backward}/r_{forward}$) [3], which is equal to 1 in equilibrium, ranges from 4×10^{-4} (for 450 °C) to 4×10^{-2} (for 700 °C). As r was very close to zero for all conditions, the measured rate (net reaction rate) was considered equal to the forward reaction rate.

Additional experiments were performed over Rh/A catalysts subjected to two different in situ pretreatments: (i) reduction at 700 °C in pure H_2 (80 ml/min) during 1 h, and (ii) oxidation at 700 °C in pure O_2 (80 ml/min) during 1 h.

The reaction was carried out in the described flowing mixture at temperatures ranging from 500 to 700 °C and a space velocity of 1.2×10^5 ml/h/g_{cat}. In order to study the catalytic performance of Rh atoms in the oxidation state reached during the pretreatment, the activities were measured immediately after (1 min) the admission of the gas mixture.

2.2.2. Diagnostic tests for mass transfer limitations

Absence of external and internal mass transfer limitations was assured. The interparticle limitation tests, performed at a space velocity of 6×10^5 ml/h/g_{cat}, showed equal conversions for flow rates above 200 ml/min, indicating that no external limitations exist at those conditions. At a selected flow rate of 300 ml/min, the absence of intraparticle limitations was verified along the whole particle size range analyzed (73–380 μm). In summary, mass transfer limitations and diffusion rate-controlling regime were fully excluded for the conditions selected to perform catalytic tests, i.e. a flow rate of 300 ml/min and a particle size range of 104–180 μm.

2.2.3. Analysis of reactants and products

The effluents were analyzed by online gas chromatography using a 60/80 Carboxen-1000 stainless steel column (Supelco) and a thermal conductivity detector installed in a gas chromatograph (Perkin Elmer, Autosystem XL). The sequence of analyses was performed in periods of 15 min, allowing the quantification of hydrogen, carbon monoxide, methane, carbon dioxide and water concentrations.

The methane conversion (X_{CH_4}), the yield (Y_i) and selectivity (S_i) of the product i were calculated as follow:

$$X_{CH_4} = \frac{F_{CH_{4,inlet}} - F_{CH_4}}{F_{CH_{4,inlet}}} \quad (1)$$

$$Y_i = \frac{(F_i - F_{i,inlet})|\nu_{CH_4}|}{F_{CH_4,inlet}\nu_i} \quad (2)$$

$$S_i = \frac{(F_i - F_{i,inlet})|\nu_{CH_4}|}{F_{CH_4} - F_{CH_4,inlet}|\nu_i|} \quad (3)$$

where F_i and ν_i are the molar flow and the stoichiometric coefficient of the product i, respectively.

2.3. Thermodynamic calculations

Equilibrium compositions were determined by minimizing the total Gibbs energy of the gas mixture, at 1 atm and an initial composition of CO_2:CH_4:He = 5:5:90, using the HYSYS simulation software package [27]. The reaction temperature was varied between 450 and 700 °C.

2.4. Characterization of samples

N_2 (Indura S.A., >99.9%) adsorption isotherms of the samples were recorded at 77 K (temperature of liquid N_2) with a Micromeritics Gemini apparatus. Samples were previously outgassed under vacuum at 300 °C for 24 h. The surface area was calculated according to the BET method and the total pore volume (V_p) was taken at a relative pressure of 0.99. The average pore size was estimated as $2V_p$/SBET.

X-ray diffraction profiles were recorded using a Rigaku Geigerflex (Dmax II) diffractometer, operating at 40 kV and 20 mA with nickel-filtered Cu Kα1 radiation (λ = 1.5418 Å).

The ZrO_2 crystal sizes were estimated according to the Scherrer's equations:

$$d = \frac{0.94 \cdot \lambda}{B(2\theta) \cdot \cos\theta} \quad (4)$$

where B is the FWHM (full width at half maximum); λ is the X-ray wavelength; θ is the Bragg angle.

X-ray photoelectron spectra were obtained for fresh and tested samples with a Surface Science Instruments SSX-100 model 206 spectrometer equipped with a monochromatized microfocused Al X-ray source, operating at 10 kV and 12 mA. The residual pressure inside the analysis chamber was about 10^{-6} Torr. The flood gun energy was adjusted at 8 eV with a fine-meshed nickel grid placed 3 mm above the sample surface. The pass energy was 150 eV and the spot size was 1000 μm, leading to an energy resolution of 1.6 eV. The angle between the normal to the sample surface and the direction of electron collection was 55°. The binding energy scale of the spectrometer was calibrated with respect to the Au4f7/2 peak of gold fixed at 83.98 eV and the binding energies of O1s, Al2p, Zr3d, and Rh3d were referenced to the C1s band at 284.8 eV.

The peak decomposition was performed using the CasaXPS program (Casa Software, UK), assuming a 85/15 Gaussian/Lorentzian product function. In order to obtain the XPS atomic ratio between Zr3d and Al2p, the normalized intensities of Zr3d, and Al2p were calculated by multiplying the relative area of the corresponding peaks by the sensitivity factors provided by the manufacturer. The theoretical XPS $(Rh/Al)_m$ and $(Rh/Zr)_m$ atomic ratios corresponding to a monolayer dispersion of rhodium were calculated from the $(Rh/support)_b$ bulk atomic ratio, the relative photoelectron cross sections (σ_{Rh}, σ_{supp}) and the escape depths of electrons through the support (λ_{Rh}, λ_{supp}), considering the model proposed by Kerkhof and Moulijn [28]. According to this model, the catalyst consists on cubic metallic crystallites deposited over sheets of support. The thickness (t) of these sheets can be estimated from the density (ρ) and the surface area of the support:

$$t = \frac{2}{\rho_{supp} \cdot S_{BET,supp}} \quad (5)$$

When electrons with small differences in kinetic energy are studied, and thus their escape depths through the support can be considered to be equal ($\lambda_{Rh} = \lambda_{supp} = \lambda$), the XPS atomic ratio of a monolayer catalyst can be predicted by:

$$\left(\frac{Rh}{supp}\right)_m = \left(\frac{Rh}{supp}\right)_b \cdot \frac{\sigma_{Rh}}{\sigma_{supp}} \cdot \frac{\beta}{2} \quad (6)$$

where β is the dimensionless support thickness:

$$\beta\frac{t}{\lambda} \quad (7)$$

The weighted average value of these calculated ratios were used to obtain the theoretical XPS Rh/(Al + Zr) atomic ratios for mechanical mixtures. The nominal amount of rhodium in the catalysts was used for the calculation of $(Rh/support)_b$ bulk atomic ratios, considering that no evidences have been reported regarding mass loss of rhodium during the calcination treatment [29].

From the XPS surface atomic compositions, the Rh particle sizes were estimated according to the following equations [30]:

$$d = \frac{3}{2}\left(\frac{N}{A \cdot \rho}\right)\left(\frac{MW}{N_A}\right) \quad (8)$$

$$N = \left(\frac{L}{S_{BET}}\right)\left(\frac{N_A}{MW}\right) \quad (9)$$

where N is the Rh surface density (atoms/cm^2); A is the Rh surface atomic composition from XPS; ρ is the bulk density of Rh (g/cm^3); L is the Rh loading (g/g_{cat}); MW, NA, SBET are molecular weight, Avogadro's number and BET surface area, respectively.

Temperature programmed reduction (TPR) characterization of the samples was performed in a ChemBET Pulsar TPR/TPD (Quantachrome Instruments) analyzer provided with a TCD detector. The sample (150 mg, particle size range of 100–300 μm) was placed into a quartz U tube and subjected to a 5% H_2/Ar (Indura S.A., >99.99%) flow of 30 ml/min, while increasing the temperature up to 700 °C at a rate of 10 °C/min.

Carbon monoxide (Indura S.A., >99.99%) pulse chemisorption was performed at room temperature, assuming an adsorption stoichiometry of $CO/Rh_s = 1$ (CO adsorbed to surface Rh-atoms ratio). The catalyst was reduced in pure hydrogen (30 ml/min) by heating

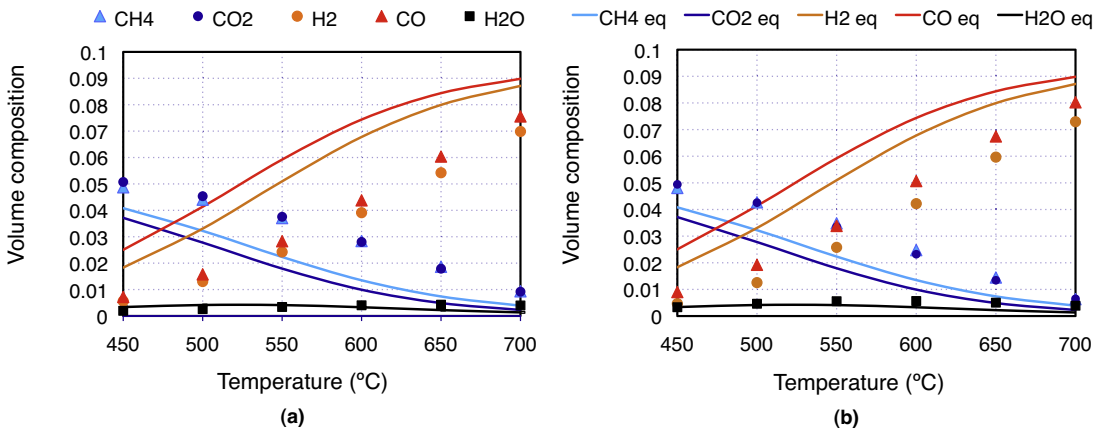

Fig. 1. Equilibrium and experimental compositions of CH_4, CO_2, H_2, CO and H_2O in dry reforming of methane as a function of temperature. (a) 1 wt.% Rh/A; (b) 1 wt.% Rh/100Z-A. Conditions: fixed bed reactor; CH_4:CO_2:He = 5:5:90 vol.%; SV = 6×10^5 ml/h/g_{cat}; 1 atm.

up to 700 °C at 10 °C/min, and keeping the sample at this temperature for 1 h. After flushing with He for 30 min, the reactor was cooled down in He. Once reached the steady state at 25 °C, a pulse (132 μl) of CO/He (9.7 vol.% CO) mixture was sequentially passed through the sample bed, until reaching saturation of CO on the sample surface. The sample was subsequently purged with He for 15 min and then, additional CO pulses were introduced until saturation. The CO adsorbed in this second sequence of pulses corresponds to the amount reversibly adsorbed in the former run and thus, must be subtracted to obtain the CO effectively chemisorbed.

3. Results

3.1. Thermodynamic calculations

The simulated equilibrium compositions are indicated as solid lines in Fig. 1. The experimental compositions (temperature ranging from 450 to 700 °C) obtained for pure and grafted catalysts are indicated by symbols. At the selected reaction conditions, the reverse water–gas shift reaction (RWGS: $H_2 + CO_2 \rightarrow CO + H_2O$) is expected to occur simultaneously with methane reforming [31]. This reaction leads to a H_2/CO ratio less than 1. At high temperature, the thermodynamic equilibrium predicts a H_2/CO ratio close to unity.

3.2. Catalytic activity measurements

3.2.1. Catalytic performance of Rh supported on pure alumina and Zr-grafted alumina

As a first step, DRM reaction was studied by using Rh catalysts supported on pure alumina and Zr-grafted alumina (results shown in Fig. 1 and Table 1). Then, isothermal catalytic tests were performed with mechanical mixtures (Fig. 2 and Table 2).

The Zr grafting over alumina surface allows improving the catalytic performance of Rh/A. The methane and CO_2 conversions in the whole temperature range (450–700 °C) are higher for Rh/100Z-A catalyst than for Rh/A: an improvement of about 15% is observed at 600 °C (Table 1). The grafted catalyst also presents higher CO and

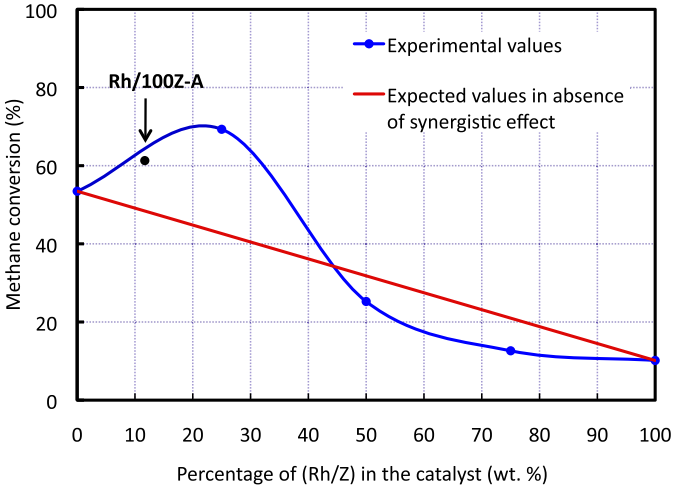

Fig. 2. CH_4 conversion as a function of the (Rh/Z) percentage in Rh/A + Rh/Z mechanical mixtures. The black dot corresponding to the Rh/100Z-A catalyst (equivalent to a mixture with 12 wt.% of Rh/Z).

H_2 yields, particularly at temperatures in the range of 600–700 °C. The lower H_2 concentration, with respect to CO, and the water formation may result from the reverse water–gas shift reaction. The addition of ZrO_2 might slightly promote this reaction, leading to a marginally higher water formation observed for the grafted sample. Since RWGS reaction may occur simultaneously, yields and selectivities were calculated based only on the conversion of methane, which will be the focus of the analysis and discussion hereafter.

The H_2/CO ratio increases with the temperature, up to values close to 1 at 700 °C. On the other hand, CO_2 and CH_4 conversions also increase (Table 1), which is consistent with the thermodynamic calculations and with the previously reported data [14].

The stability of pure and grafted catalysts was tested under drastic conditions (2×10^6 ml/h/g_{cat}, 700 °C). A stationary state is reached after 1 h of reaction. The activities remain constant for

Table 1
Catalytic activity of Rh/A and Rh/100Z-A in dry reforming of methane: CH_4 conversion, H_2 and CO yields.[a]

Catalyst	% CH_4 conversion			% H_2 yield (% CO yield)			H_2/CO molar ratio		
	450 °C	600 °C	700 °C	450 °C	600 °C	700 °C	450 °C	600 °C	700 °C
Rh/A	7.7	46	82	5.3(6.8)	37(41.1)	66(71.7)	0.78	0.90	0.92
Rh/100Z-A	8.9	53	88	4.4(8.5)	40(48.2)	69(75.8)	0.52	0.83	0.91

[a] Conditions: CH_4/CO_2/He = 5/5/90 vol.%, SV = 6×10^5 ml/h/g_{cat}, results obtained after 1 h.

Table 2
Catalytic activity of mechanical mixtures in dry reforming of methane, as a function of the percentage of Rh/Z in the mixture.[a]

Mechanical mixture	Rh/A	75Rh/A + 25Rh/Z	50Rh/A + 50Rh/Z	25Rh/A + 75Rh/Z	Rh/Z
CH_4 conversion (%)[b]	53	69 (43)	25 (32)	13 (21)	10
H_2 yield (%)	42	52	18	8.5	5.5
CO yield (%)	48	58	23	12	11
H_2/CO molar ratio	0.88	0.90	0.78	0.71	0.50

[a] Conditions: CH_4/CO_2/He = 5/5/90 vol.%, SV = 1.63×10^5 ml/h/g_{cat}, T = 600 °C, results obtained after 1 h.
[b] In parenthesis, the weighted average value of the conversions obtained for the single Rh/A and Rh/Z catalysts.

about 4 h, and then they start to decrease very slightly. After 25 h, Rh/A and Rh/100Z-A catalysts present 94 and 95% of their initial activities, respectively.

3.2.2. Catalytic performance of Rh/A + Rh/Z mechanical mixtures

Results obtained for mechanical mixtures are presented in Table 2. Rh/Z catalyst shows very low activity: methane conversion is only 10% at 600 °C and H_2 and CO yields are 5.5% and 11.0%, respectively. On the contrary, Rh/A is about 5 times more active, presenting a methane conversion of 53%, and yields of H_2 and CO of 42% and 48%, respectively.

If the reaction is assumed to be zero order and the space velocity is kept constant, the conversion depends on the composition of the mixture used as catalyst. Hence, the expected conversion of a mechanical mixture would correspond to the weighted average value of the conversions obtained for Rh/A and Rh/Z, as single catalysts. The straight line in Fig. 2 represents these values, which are also presented in parenthesis in Table 2. An important synergistic effect is observed for the mechanical mixtures with high Rh/A contents. Among tested mixtures, 75Rh/A + 25Rh/Z exhibits the maximum in methane conversion (69%), H_2 yield (52%) and CO yield (58%).

The conversion obtained with the grafted catalyst was included in Fig. 2 for a first comparison with the catalytic performances of mechanical mixtures. The surface concentration of ZrO_2 in the 100Z-A support was estimated in 12% by XPS analysis. Then, Rh/100Z-A is comparable with a mechanical mixture containing 12 wt.% of Rh/Z, when assuming that rhodium is deposited on ZrO_2 and γ-Al_2O_3 in proportion to their surface concentrations on the grafted support. The activity of Rh/100Z-A seems to be similar to what experimental results predict for a mechanical mixture with 12 wt.% of Rh/Z. This indicates that the same cooperative effect observed in the mechanical mixtures might also occur in the grafted catalyst, between Rh/A and Rh/Z phases in good contact composing the surface.

3.2.3. Effect of the pretreatment on the catalytic activity of Rh/A

Results of catalytic tests performed with pre-oxidized and pre-reduced Rh/Al catalysts are presented in Fig. 3. As the methane conversion was measured after a very short time of reaction, values are considered as initial conversions of the oxidation state of Rh reached immediately after the pre-treatment (namely fully oxidized and fully reduced). The initial conversion is very similar for both catalysts at all reaction temperatures, and it increases from about 11% at 500 °C to 76% at 700 °C. The activation energies corresponding to the initial reaction rates are 59.8 kJ/mol and 62.4 kJ/mol, for the pre-oxidized and pre-reduced Rh/A catalysts, respectively.

3.3. Textural properties

After grafting a theoretical monolayer of ZrO_2, the support loses about 8% of its BET surface area, and after Rh impregnation and the subsequent calcination at 700 °C, the loss in surface area is about 18% (Table 3). The pore volume also decreases and the pore size increases slightly.

Table 3
Textural properties of pure and grafted alumina and the Rh-supported catalysts.

Sample	SBET (m^2/g)	Pore volume (cm^3/g)	Pore size (nm)
γ-Al_2O_3	72	0.25	6.9
100Z-A	66	0.20	6.2
Rh/A	59	0.23	7.8
Rh/100Z-A	54	0.20	7.3

Table 4
XPS atomic ratios, binding energy and proportion of Rh^0, Rh_2O_3 and RhO_2 species for Rh supported on grafted alumina catalyst.

Sample	Rh/100Z-A	
	Fresh	Tested
I_{Rh}/I_{Al+Zr}	0.009	0.008
I_{Zr}/I_{Al+Zr}	0.086	0.081
RhO_2 (BE ~ 309.5 eV)	73%	32%
Rh_2O_3 (BE ~ 308.5 eV)	20%	0
Rh^0 (BE ~ 307 eV)	7%	68%

3.4. XPS measurements

The binding energies of Zr3d (around 182.2 eV) and Al2p (around 74.4 eV) photoelectrons from the grafted support respectively correspond to those of the pure ZrO_2 and γ-Al_2O_3 [32], and remain unchanged after Rh deposition.

The XPS atomic ratios of Rh and Zr relative to the atoms of grafted support (Al + Zr), namely XPS Rh/(Al + Zr) and XPS Zr/(Al + Zr) atomic ratios, remain unchanged after reaction (Table 4).

The decomposition of XPS Rh3d peaks into 3 characteristic doublets with the 3d5/2 components at 307, 308.5 and 309.5 eV can be associated with the presence of Rh^0, Rh_2O_3 and RhO_2 species, respectively [33]. The surface proportions of those species were

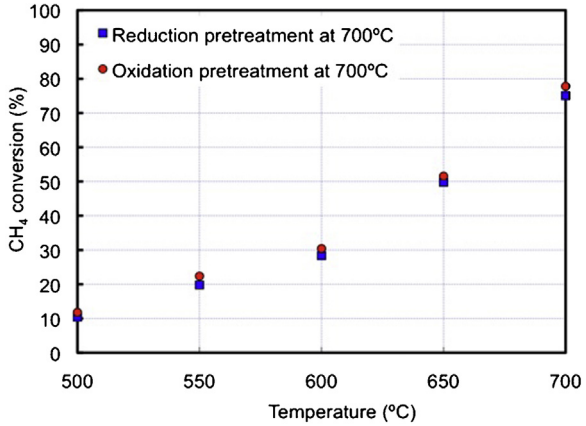

Fig. 3. Initial CH_4 conversion as a function of the temperature, for Rh/A catalysts subjected to different pretreatments. Results obtained 1 min after the admission of the gas mixture.

Table 5
XPS analysis. Binding energies of photoelectrons for Rh/A + Rh/Z mechanical mixtures.

Mixtures	Rh/A		75Rh/A + 25Rh/Z		50Rh/A + 50Rh/Z		25Rh/A + 75Rh/Z		Rh/Z	
	Fresh	Tested	Fresh	Tested	Fresh	Tested	Fresh	Tested	Fresh	Tested
O1s	531.2	531.0	531.2	531.1	531.3	531.0	531.3	531.3	531.1	529.9
Rh3d	310.1	308.8	309.9	309.1	308.9	309.0	308.5	308.2	308.5	308.1
Zr3d	–	–	181.8	182.6	182.1	182.2	182.1	182.1	182.3	182.3
Al2p	74.6	74.5	74.5	74.9	74.6	74.9	74.7	74.8	–	–

Table 6
XPS atomic ratios for Rh/A + Rh/Z mechanical mixtures.

Mixtures	Rh/A		75Rh/A + 25Rh/Z		50Rh/A + 50Rh/Z		25Rh/A + 75Rh/Z		Rh/Z	
	Fresh	Tested	Fresh	Tested	Fresh	Tested	Fresh	Tested	Fresh	Tested
I_O/I_{Al+Zr}	1.6	1.7	1.9	1.8	2.0	1.8	1.8	1.8	2.4	2.3
I_{Rh}/I_{Al+Zr}	0.005	0.005	0.007	0.006	0.009	0.007	0.012	0.008	0.037	0.026
I_{Zr}/I_{Al+Zr}	–	–	0.03	0.02	0.08	0.08	0.20	0.20	1.0	1.0

Table 7
XPS atomic composition of Rh^0, Rh_2O_3 and RhO_2 in Rh/A + Rh/Z mechanical mixtures.

Mixtures	Rh/A		75Rh/A + 25Rh/Z		50Rh/A + 50Rh/Z		25Rh/A + 75Rh/Z		Rh/Z	
	Fresh	Tested	Fresh	Tested	Fresh	Tested	Fresh	Tested	Fresh	Tested
%RhO_2 (309.5 eV)	77	48	68	47	56	40	52	31	11	2
%Rh_2O_3 (308.5 eV)	19	44	27	41	39	41	25	42	81	53
%Rh^0 (307 eV)	4	8	5	12	5	20	23	27	8	45

quantified before and after catalytic test (Table 4). The amounts of RhO_2 and Rh_2O_3 decrease after reaction, while the amount of metallic Rh increases significantly.

The binding energies measured in mechanical mixtures are presented in Table 5. The binding energy of Zr3d (182.2 eV) is nearly the same for all fresh samples, indicating the presence of ZrO_2. An increase (0.8 eV) is observed after the catalytic test for the 75Rh/A + 25Rh/Z mixture. The binding energy of Al2p (74.4 eV) is about the same for all fresh samples indicating the presence of γ-Al_2O_3. The binding energy of O1s remains unchanged for all mixtures, both before and after catalytic test.

The binding energy of Rh3d is higher for fresh Rh/A (310.1 eV) than for fresh Rh/Z (308.5 eV). After catalytic test, the Rh3d binding energy decreases for both single catalysts (in 1.3 eV for Rh/A and 0.4 eV for Rh/Z), it decreases in 0.8 eV for 75Rh/A + 25Rh/Z, it remains unchanged for 50Rh/A + 50Rh/Z, and it slightly decreases (in 0.3 eV) for 25Rh/A + 75Rh/Z.

The XPS atomic ratios are presented in Table 6. The XPS O/(Al + Zr) atomic ratio is higher for Rh/Z (2.3 eV) and remains unchanged after reaction for all samples. It can be noted that the XPS Rh/(Al + Zr) atomic ratio increases with the Rh/Z content. After catalytic test, this ratio remains nearly unchanged for the Rh/A and 75Rh/A + 25Rh/Z catalysts, it slightly decreases for 50Rh/A + 50Rh/Z and it significantly decreases for 25Rh/A + 75Rh/Z and Rh/Z. The greatest percentage decrease is reached for the Rh/Z single catalyst.

In Fig. 4, the theoretical XPS $Rh/(Al+Zr)_m$ atomic ratio, calculated assuming a monolayer dispersion of Rh [28], was plotted along with the experimental XPS $Rh/(Al+Zr)_{exp}$ atomic ratio versus the $Rh/(Al+Zr)_b$ bulk ratio. For higher contents of Rh/Z in the mixture, the $Rh/(Al+Zr)_b$ bulk ratio increases and the total surface area decreases due to the lower area of Rh/Z (~5 m^2/g). This leads to a non-linear increase of the XPS $Rh/(Al+Zr)_m$ and $Rh/(Al+Zr)_{exp}$ curves. It is observed that the amount of surface Rh atoms on the single catalysts (Rh/A and Rh/Z) is significantly lower than the amount to be expected for a monolayer dispersion of rhodium over the support. This difference is more significant in the mechanical mixtures. No migration or sintering of Rh atoms is expected during the mixture preparation, which does not include a calcination step. Then, the more important difference between XPS $Rh/(Al+Zr)_{exp}$ and $Rh/(Al+Zr)_m$ atomic ratios in mechanical mixtures may mean that the mixtures are not perfectly homogeneous and there is a higher concentration of Rh/A at the surface, contributing with a lower XPS (Rh/support) atomic ratio.

Table 7 shows that the fresh Rh/A catalyst exhibits the highest amount of fully oxidized rhodium (RhO_2 = 77%). After catalytic test, a decrease in the surface atomic percentage of RhO_2 (to 48%) is observed, whereas the percentages of Rh_2O_3 and Rh^0 increase from 19% to 44% and from 4% to 8%, respectively. Rh species are significantly more easily reduced in the Rh/Z catalyst. Moreover, a high fraction of Rh in Rh/Z is already partially reduced before the reduction treatment (81% of Rh_2O_3 and 8% of Rh^0). For this catalyst, 45% of the rhodium is in metallic state after reaction.

The Rh surface of 75Rh/A + 25Rh/Z fresh sample corresponds mainly to RhO_2 and Rh_2O_3. The surface atomic percentage of Rh^0 is

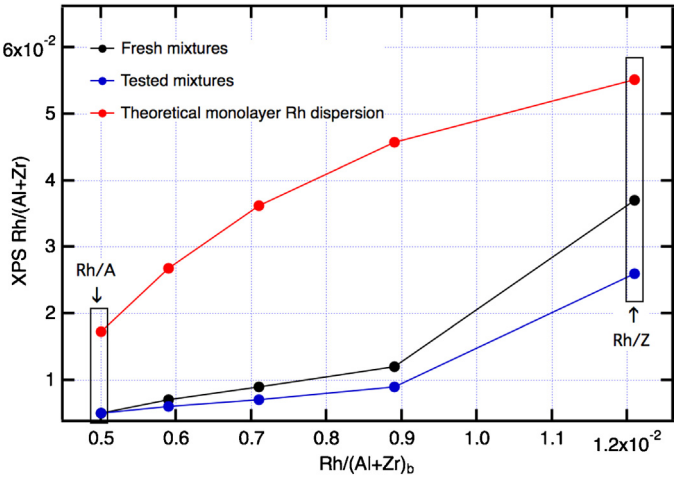

Fig. 4. XPS Rh/(Al + Zr) atomic ratio as a function of the bulk composition for Rh/A + Rh/Z mechanical mixtures. Theoretical XPS atomic ratios obtained according to Kerkhof and Moulijn [28].

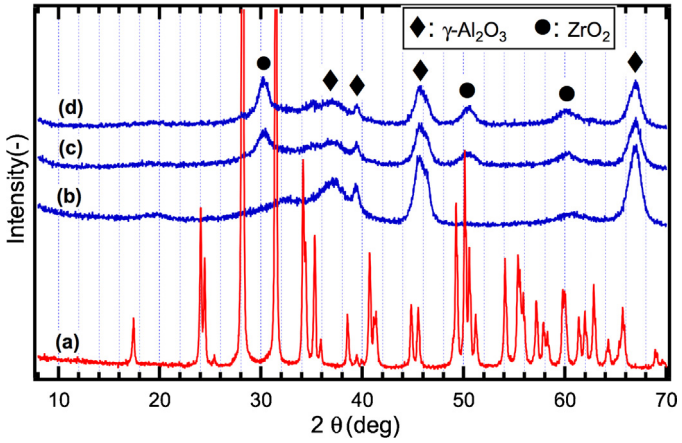

Fig. 5. XRD spectra of (a) ZrO_2, (b) γ-Al_2O_3, (c) 100Z-A and (d) Rh/100Z-A.

only 5%. For the tested 75Rh/A + 25Rh/Z mixture, rhodium is highly oxidized and only 12% corresponds to Rh^0. This mixture presents almost the same surface atomic percentage of RhO_2 (47%) as the Rh/A catalyst (48%), even though 25% of the mixture corresponds to the Rh/Z catalyst having only 2% of RhO_2. This suggests that in the mixtures, Rh/A promotes the oxidation of rhodium over Rh/Z.

The XPS analysis was not performed in situ. Indeed, after the catalytic test, the samples were cooled down to room temperature under inert gas flow, so that any possible oxidation of the catalyst by exposure to air, during its transfer into the XPS machine, is expected to be very low and concerning the most external surface layer. Considering that all (>95%) detected electrons come from within 3λ of the surface, the sampling depth of Rh3d electrons is 5.6 nm and therefore, we can estimate that about 5 molecular layers of the external surface are analyzed by XPS. Additionally, the RhO_x surface concentration (measured after the reaction) reaches values up to 90%, which indicates that the oxidized species are not only present in the outermost layer of the analyzed surface, but also in the deeper surface layers. This confirms that the possible oxidation by transferring the sample to the analyzer would not contribute significantly to the formation of the RhO_x species detected by XPS.

Furthermore, the XPS analysis may involve a reduction associated with the exposure to ultra-high vacuum conditions (10^{-5} Torr). Then, if some oxidized rhodium species were formed in the outer layer, they would be re-reduced at this stage.

3.5. XRD analysis and CO chemisorption

The XRD spectra of zirconia, alumina, 100Z-A and Rh/100Z-A are shown in Fig. 5. For the non-modified alumina support, a broad diffraction peak with two maxima at $(2\theta) = 32$ and 37.5° is observed, along with two peaks at 46 and 67°, all characteristic of the γ-Al_2O_3 phase and corresponding to the (2 2 0), (3 1 1), (4 0 0) and (4 4 0) planes, respectively. Three peaks, at $(2\theta) \approx 30.2$, 50.2 and 60°, characteristic of the tetragonal ZrO_2 phases are observed for the modified support (100Z-A). The spectrum of zirconia indicates that the monoclinic phase ($(2\theta) \approx 24$, 28.2, 31.5 and 41°) is predominant in this oxide, even though tetragonal phases are also present. For Rh/100Z-A, only the reflections due to the support are observed.

The average sizes (d) of rhodium and zirconia crystallites, obtained from XRD, XPS and CO-chemisorption analyses, are presented in Table 8. The size of the grafted zirconia crystallites increases about 10% after impregnation with Rh (Table 8), which results from the particle sintering during the calcination treatment at 700 °C. Rhodium particles over grafted alumina present the smallest sizes, while the largest Rh particles are those supported on

Table 8
Dispersion (D) and size (d) of Rh and ZrO_2 supported particles, calculated by CO-chemisorption, XPS and XRD.

Sample	CO-chemisorption		XPS	XRD
	D_{Rh} (%)	d_{Rh} (nm)	d_{Rh} (nm)	d_{ZrO_2} (nm)
Rh/A	31	3.3	3.9	–
Rh/Z	6	18.3	16.3	42.8 (monoclinic) 20.0 (tetragonal)
Rh/100Z-A	37	2.9	2.6	6.6 (tetragonal)
100Z-A	–	–	–	4.8 (tetragonal)

ZrO_2. The values obtained by CO-chemisorption are similar to those estimated from the XPS surface atomic compositions.

The measures of rhodium dispersion in the mechanical mixtures were also obtained by CO-chemisorption, and they match the weighted averages of Rh dispersions in single catalysts. For instance, a rhodium dispersion of 24% was measured by CO-chemisorption for the 75Rh/A + 25Rh/Z, while the average of Rh dispersions in Rh/A and Rh/Z is 25%.

3.6. TPR analysis

Fig. 6 shows the TPR profiles of Rh/A, Rh/Z, and 75Rh/A + 25Rh/Z samples. The peak at low temperature, attributed to the isolated RhO_x particles presenting a weak interaction with the support [18,19], appears at 120 °C for the Rh/A catalyst. For Rh/Z, the peak at low temperature appears at 110 °C with a higher intensity. For 75Rh/A + 25Rh/Z mixture, a small peak is observed at about 115 °C. Its area corresponds to 89% of the expected area from the contribution of Rh/A (75 wt.%) and Rh/Z (25 wt.%) catalysts composing this mixture. This means that some isolated RhO_x particles become harder to reduce when the catalysts are mixed.

The H_2 consumption in the case of TPR of the 75Rh/A + 25Rh/Z mixture cannot be compared with the theoretical value expected for a total reduction of Rh. In fact, the total H_2 consumed corresponds to the reduction of only a fraction of all rhodium contained in the sample, which is not fully reduced at 700 °C.

A broad peak appears at higher temperatures (200–600 °C), corresponding to hardly reducible Rh species [18,19]. The amount of these hardly reducible species increases in the order Rh/Z < Rh/A < 75Rh/A + 25Rh/Z. It is noteworthy that the broad peak shifts toward lower temperatures for the mechanical mixture.

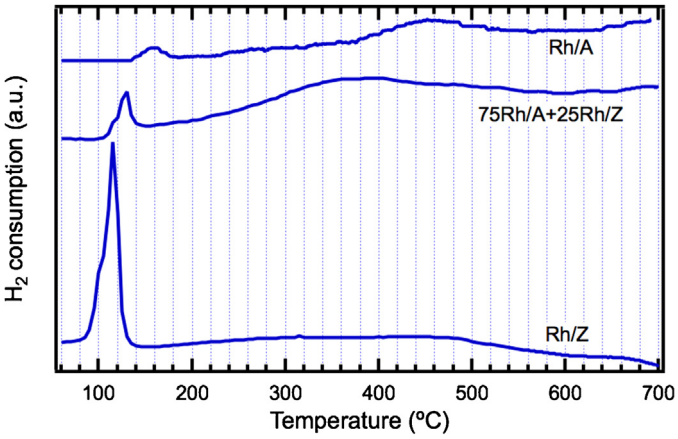

Fig. 6. TPR profiles obtained for Rh/Z, Rh/A and 75Rh/A + 25Rh/Z mechanical mixture catalysts.

Table 9
XPS atomic composition of Zr and Al in the support of mechanical mixtures.

Mechanical mixtures	% surf Rh/Z	% atom Zr3d (fresh)		% atom Al2p (fresh)		% atom Al2p (tested)	
		Exp	Theor	Exp	Theor	Exp	Theor
Rh/A	0	–	–	36	36	34	34
75Rh/A + 25Rh/Z	3	0.8	0.8	30	35	32	33
50Rh/A + 50Rh/Z	8	2.5	2.2	28	33	30	31
25Rh/A + 75Rh/Z	20	6.3	5.7	25	29	25	27
Rh/Z	100	24	24	–	–	–	–

4. Discussion

4.1. Morphology and interaction between surface phases

4.1.1. Rh catalyst over pure and grafted supports

From XRD and XPS analyses (Tables 4 and 8), it is shown that crystallites of tetragonal zirconia are formed on the grafted alumina support. This differs from results previously reported [32], which indicate that zirconia is easily dispersed as a monolayer on the alumina surface, for contents up to 12.9 wt.%. After grafting with Zr, a decrease in BET surface area, pore volume and pore diameter of the support is observed, indicating that the ZrO_2 crystallites are probably formed near the mouth of the alumina pores.

Although the formation of Zr—O—Al bonds is expected during the grafting of alumina, XPS analysis shows no change in the binding energy of Zr3d photoelectrons, compared to that for pure zirconia. This is consistent with the formation of ZrO_2 crystallites over alumina, where Zr—O—Al bonds would be located below the XPS sampling depth. On the other hand, the Al2p binding energies also correspond to values of pure γ-Al_2O_3, confirming that if Zr—O—Al bonds are detected by XPS, they are negligible.

After rhodium impregnation over grafted alumina (100Z-A), the XPS atomic composition of Zr shows a greater decrease than the Al atomic composition, which suggests that Rh is preferably deposited over zirconium oxide. However, no interactions between Rh and ZrO_2 or alumina seem to occur during the impregnation process, since the binding energies corresponding to both oxides remain essentially unchanged.

The Rh particles are better dispersed on the grafted catalyst than in the non-modified catalysts (Table 8). In all cases, the Rh particles are not large enough to be detected by XRD (i.e. high metal dispersion), which is mainly attributed to the low Rh content in the catalysts (1 wt.%). Indeed, the XRD detection of Rh^0, Rh_2O_3 and RhO_2, in Rh/A catalysts calcined at 700 °C, has been reported only for rhodium loadings higher than 3 wt.% [34,35].

It can be concluded that the Zr-grafting technique allows the formation of ZrO_2 crystallites on the alumina surface, rather than a ZrO_2 monolayer. The support is then formed by the grafted ZrO_2 crystallites and the uncovered alumina surface. Over this modified support, the rhodium can be deposited with a higher dispersion than over pure alumina, and without forming mixed phases with alumina and/or zirconia. Thus, the grafted catalyst contains Rh/A and Rh/Z in good contact and it can be represented as a mixture of both catalysts separately prepared.

4.1.2. The solid state of the mechanical mixtures

The binding energies for Zr3d (182.2 eV) and Al2p (74.4 eV) indicate the sole presence of ZrO_2 and γ-Al_2O_3 species, respectively. This has been confirmed by XRD analysis. Similar binding energies were observed after the catalytic test. Thus, no new phases seem to be formed between γ-Al_2O_3 and ZrO_2 during the preparation of mixtures or during the reaction. However, we cannot completely rule out the existence of slight interactions at the outermost layer of the particles in mixture, involving undetectable changes in the binding energies of Zr3d and Al2p photoelectrons. The decrease of the Rh3d binding energy (from 310.1 to 308.5 eV) when the content of Rh/Z in mixture increases is mainly attributed to the contribution of the lower oxidation state of Rh over zirconia.

The XPS Rh/(Al + Zr) atomic ratio in the Rh/A catalyst remains unchanged after the catalytic test. A significant decrease of this ratio is only observed for samples with high Rh/Z contents (Table 6). This may be attributed to the sintering of rhodium in Rh/Z single catalyst.

The Rh/Z surface area is very low (~5 m^2/g) and equivalent to 5% of the Rh/A surface area. Therefore, the surface percentage of Rh/Z in the mechanical mixtures was used (instead of the mass percentage) to calculate the theoretical Al and Zr atomic compositions in the mechanical mixtures, as an average of the experimental values corresponding to the single catalysts. Results are presented in Table 9. The XPS Zr3d atomic compositions obtained by analyzing fresh mixtures, agree with the calculated values. In the case of the Al2p atomic compositions, the theoretical and experimental values for fresh samples differ in less than 5%. In addition, the Al2p atomic compositions remain unchanged after catalytic test. The results confirm that if any interaction exists between ZrO_2 and γ-Al_2O_3 this is minimal. Moreover, no formation of mixed phases between ZrO_2 and γ-Al_2O_3 was detected during the grafting process, although this technique provides highly favorable conditions for bond formation.

Although XPS atomic ratio gives reliable information about dispersion changes of Rh particles during the reaction, it is important to note that the increase of XPS Rh/(Al + Zr) atomic ratio with the Rh/Z content in the mixture cannot be interpreted as an increment in Rh dispersion. In fact, the dispersion of Rh on zirconia is lower than over alumina, so that Rh/Z contributes to reduce Rh dispersion in the mixtures. However, the increase of the Rh/Z content also leads to a significant decrease in the total surface area of the mixture (as the specific surface area of ZrO_2 is very small compared to that of γ-Al_2O_3). This causes an increase of the atomic surface concentration of Rh, even though its dispersion decreases.

The increasing character of the XPS $Rh/(Al + Zr)_m$ atomic ratio curve, as a function of the bulk composition of the mixtures, seems to confirm this observation (Fig. 4). The XPS $Rh/(Al + Zr)_{exp}$ atomic ratios, obtained for fresh and tested mixtures, are significantly lower than the atomic ratios calculated for a monolayer dispersion of rhodium, indicating that there is no rhodium enrichment of the surface during the mixture preparation and/or during the reaction. Therefore, the migration of Rh between the two catalytic components of the mixture seems to be completely excluded.

It is important to underline that for the 75Rh/A + 25Rh/Z mixture (sample with the highest activity), the XPS Rh/(Al + Zr) atomic ratio remains unchanged after the catalytic test. The latter may imply that: (i) there is no formation of a new oxide phase between the supports; (ii) there is neither migration of Rh atoms from one catalytic component to the other, nor a significant sintering of Rh particles during the reaction.

Since oxygen is present in all phases (RhO_x, γ-Al_2O_3 and ZrO_2), the variation of the XPS O/(Al + Zr) atomic ratio does not give a relevant information about the solid surface of the sample, and therefore not about its catalytic activity.

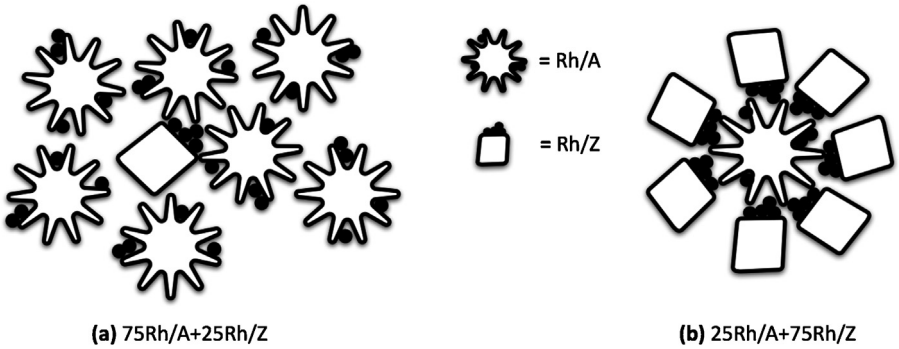

Scheme 1. Representation of the mechanical mixtures between Rh/A (Rh is highly dispersed) and Rh/Z (Rh is poorly dispersed) catalysts. In (a), the contacts between Rh atoms (●) of Rh/Z and the alumina surface of Rh/A are lower, while these contacts are higher in (b).

All previous results allow us to conclude that the mixtures contain Rh/A and Rh/Z, as separated catalysts in good physical contact.

The TPR analysis provides some evidences of Rh-support interactions in the mixtures. For the 75Rh/A + 25Rh/Z sample, a high amount of hardly reducible Rh species (broad peak at 200–600 °C) was observed, while the peak attributed to the more easily reducible RhO_x particles, preferably present in Rh/Z (at 110 °C), is 10% smaller than the expected from the contribution from single catalysts (Fig. 6). This indicates that the reducibility of Rh species over zirconia might decrease because of the mixing process.

The migration of Rh atoms from one catalyst to the other, during reaction, was discarded by XPS of tested samples. Thus, one explanation could be that the rhodium deposited over zirconia interacts with the exposed surface of alumina on Rh/A, and such interaction would occur at the contact points between the mechanically mixed Rh/Z and Rh/A catalysts. If this interaction exists, it should lead to an increase of the XPS Rh/(Al + Zr) atomic ratio. However, during the reaction an important decrease of this ratio is also expected from the sinterization of Rh over zirconia. The simultaneous occurrence of both phenomena agrees with the very slight decrease of XPS Rh/(Al + Zr) atomic ratio for 75Rh/A + 25Rh/Z and 50Rh/A + 50Rh/Z mixtures (Table 6). The decrease in the XPS Rh/(Al + Zr) atomic ratio is higher for 25Rh/A + 75Rh/Z and even higher for Rh/Z, confirming the strong sintering process occurring on Rh/Z.

4.1.3. The oxidative role of Rh/A and the role of Rh/Z as reduction promoter

The surface area of Rh/Z is significantly lower than Rh/A surface area. Thus, the interactions between alumina support and the less dispersed Rh over zirconia should be magnified at high amounts of Rh/Z in the mixture, as shown in Scheme 1. This is expected to occur in the 25Rh/A + 75Rh/Z mixture, where the total surface area of Rh/Z approaches the surface area value of the Rh/A, favoring a high number of contacts between both catalysts.

It has been suggested that calcination at high temperature leads to RhO_x species strongly bound to alumina, which are hardly reducible by the hydrogen molecules in gas phase [18]. Our results seem to support the evidence of such results. The TPR profile for the Rh/A catalyst shows a broad peak at high temperatures (200–600 °C), as seen in Fig. 6. However, this peak is bigger and shifts toward lower temperatures in the TPR profile of 75Rh/A + 25Rh/Z. This might imply that Rh/Z is promoting the reduction of the hardly reducible Rh species over alumina, including part of the non-reduced rhodium in Rh/Al at 700 °C. A higher reducibility of rhodium can be promoted by facilitating the supply of hydrogen. Therefore, the mechanism of reduction that may be present in the mixture would be the dissociative adsorption of H_2 molecules over Rh/Z and the subsequent migration of hydrogen atoms to the Rh/A phase, promoting its reduction. The migration of hydrogen may occur via a spillover mechanism, considering the close contact between both catalytic components in the mixtures [36,37].

Under reaction conditions, the promotion effect between the phases coexisting in the mechanical mixtures takes place in a different way. The XPS analysis indicates that the presence of Rh/A promotes the oxidation of Rh over zirconia during the reaction. Though the Rh/Z catalyst remains almost completely reduced when used as a single catalyst, it achieves a high oxidation state in the presence of Rh/A, particularly in the 75Rh/A + 25Rh/Z and 50Rh/A + 50Rh/Z mixtures. As Rh/A and Rh/Z catalysts in close contact are present in the mixtures, it can be suggested that Rh/A promotes the oxidation of Rh/Z by providing oxygen species (from the activation of CO_2) that subsequently migrate to Rh/Z. These aspects are further discussed in the next section.

4.2. Catalytic performance of the Rh/A + Rh/Z mixtures and Rh/100Z-A catalyst

Physico-chemical characterization of catalysts clearly suggests that the synergistic effect observed in the mechanical mixtures can be explained by a catalytic cooperation effect between Rh/A and Rh/Z separated catalysts having a good contact. The results for the mixtures with low Rh/Z contents (those presenting a positive synergy) allow excluding the formation of new phases between γ-Al_2O_3 and ZrO_2 and the increase in Rh dispersion during the reaction, as possible causes of the increased activity (Fig. 4).

From XPS analysis, two important observations can be noted: (i) the Rh/A catalyst promotes the oxidation of rhodium over zirconia during reaction and (ii) a high surface concentration of oxidized rhodium is required to achieve a high activity in dry reforming of methane. Indeed, the Rh/Z catalyst shows a very low activity, having the highest amount of reduced Rh. The best catalytic performance is observed for the mechanical mixture with 75% of Rh/A, which reaches a very high atomic percentage of RhO_x (88%). This value is similar to the percentage of oxidized rhodium in the single Rh/A catalyst (92%), even though the mixture contains 25% of Rh/Z having only 55% of RhO_x. This shows that Rh/A promotes the oxidation of the rhodium located on Rh/Z, when both catalytic particles are in physical contact.

The RhO_x atoms measured by XPS can be mainly attributed to the oxidation during the catalytic reaction, even if a very slight oxidation of rhodium surface might occur during the transfer of the samples toward the XPS machine. In any case, the analysis of Rh oxidation state presented here is focused on the tendency of the results obtained with different catalysts, not on the absolute values, and it clearly reveals a promotion of Rh oxidation in the mixtures.

If the migration of oxygen species on the surface of particles in good contact is accepted, we can propose a mechanism explaining

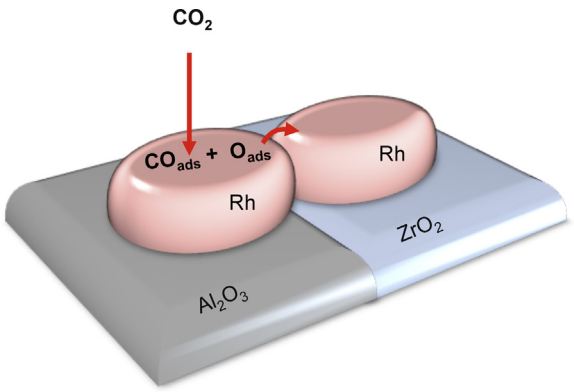

Scheme 2. Oxidation of rhodium by O(ads) activated species.

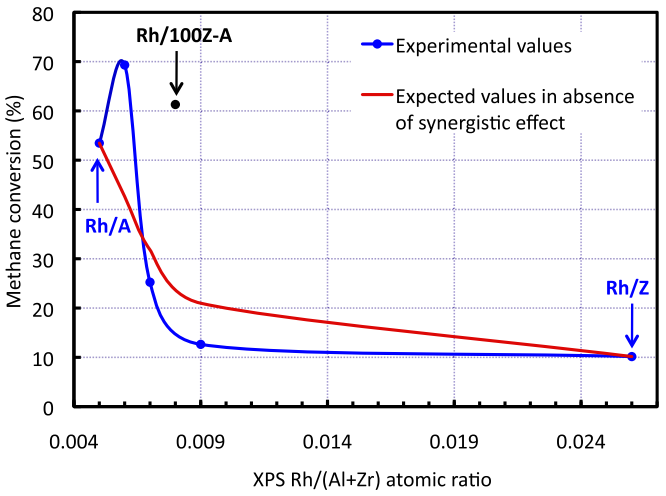

Fig. 7. CH_4 conversion as a function of the XPS Rh/(Al + Zr) atomic ratio in the mechanical mixtures. The black dot corresponding to the Rh/100Z-A catalyst.

the promotion of Rh oxidation (Scheme 2). It has been shown experimentally that CO_2 is dissociatively adsorbed on the metallic Rh sites of the Rh/A catalyst and that the monoatomic oxygen species formed by the dissociation ($CO_2 \rightarrow CO + O(ads)$) exhibit a strong oxidant character, being able to maintain an important amount of Rh sites in a high oxidation state during reaction [38–41]. Those O(ads) species may migrate to the Rh/Z catalysts promoting the oxidation of Rh in it. Besides, the O(ads) species could be able to oxidize some strongly adsorbed molecules on the catalysts that cause its deactivation, thus increasing the resistance to carbon formation.

For mixtures with high Rh/Z contents, the low amount of Rh/A is not able to promote the oxidation of Rh during the reaction. For the mixture with 75% of Rh/Z, the percentage of metallic Rh (27%) is higher than the expected from the contribution of Rh/Z, which indicates that the role of Rh/Z in promoting the Rh reduction becomes more significant than the oxidative role of Rh/A. The low fraction of oxidized Rh results in a low activity of this mixture, being similar to that observed for the single Rh/Z catalyst. Not only the rhodium over zirconia remains highly reduced, but also Rh/Z is able to activate hydrogen species that promote a further reduction of the Rh over alumina, thus leading to the slight negative effect observed in Fig. 2 for the mixtures with high amounts of Rh/Z.

The results show that a high activity of Rh supported catalysts in dry reforming of methane can be obtained when both oxidized and reduced Rh sites are present in the right proportion. The surface distribution of Rh oxidation states in the 75Rh/A + 25Rh/Z mixture seems to be more favorable for the reaction than the one reached for the single catalyst, thus explaining the synergistic effect.

It is generally accepted that the C—H bond activation of methane (the rate-determining step of CH_4 dry reforming) occurs over metallic Rh sites [3,4]. Our results strongly suggest that the CH_4 activation on the Rh^0 sites would be better conducted when RhO_x sites are also present in the surface, probably via an oxygen-assisted dissociation pathway (Scheme 3), which has been already proposed for the C—H bond activation over Rh and other metals such us Pd [42,43].

The importance of the presence of oxidized rhodium on the surface was confirmed by the additional catalytic experiments performed with pre-oxidized and pre-reduced Rh/A catalysts (Fig. 3). According to the TPR analysis (Fig. 6), a great part of Rh is expected to be reduced during the reduction pretreatment at 700 °C. Besides, it is accepted that Rh is fully oxidized after an equally drastic oxidation pretreatment. As the catalytic activity was measured only after one minute of reaction, the calculated methane conversions correspond to the initial values at the different oxidation states of Rh. Results show that conversion values are similar for pre-oxidized and pre-reduced catalysts, suggesting that the presence of oxidized Rh is important in dry reforming of methane and that methane activation may occur not only on the Rh^0–Rh^0 pair of sites, but also on Rh^0–RhO_x. These results are in disagreement with previous studies on methane activation, according to which the metal surface may be covered by O species that do not participate in the reaction [3,44]. The present results strongly suggest that those O species can oxidize the Rh surface and that RhO_x sites generated may directly participate in the reaction mechanism.

An enhancement in the catalytic activity is also obtained for the Rh/100Z-A grafted sample, with respect to the single Rh/A and Rh/Z catalysts. The grafted catalyst is essentially formed by well-dispersed particles of Rh/A and Rh/Z in good contact, so the high activity can be attributed to the same cooperative effect observed in the mechanical mixtures.

In Fig. 2, the activity of Rh/100Z-A and a mixture having 12% of Rh/Z were compared, assuming that rhodium is deposited on the support proportionally to the γ-Al_2O_3 and ZrO_2 concentrations. However, the XPS analysis shown that Rh is preferably deposited over zirconium oxide than over alumina (Section 4.1.1), so a mixture containing more Rh/Z can better represent the Rh/100Z-A catalyst. This is confirmed in Fig. 7, where the CH_4 conversion is plotted as a function of the XPS Rh/(Al + Zr) atomic ratio. The synergistic effect in the mixtures is observed as in Fig. 2, but the dot corresponding to Rh/100Z-A shifts toward a position between the mixtures with 50 and 75% of Rh/Z. The grafted sample is actually much more active than its equivalent mechanical mixture.

It is noteworthy that grafted ZrO_2 has a tetragonal structure, while bulk zirconia exhibits monoclinic and also tetragonal phases.

According to the quantitative analysis of the bulk ZrO_2 diffraction pattern (Table 8), the size of monoclinic crystals is around 2 times the size of tetragonal crystals, and the surface area per unit volume of monoclinic crystals is 53% lower. This means that the tetragonal crystallites contribute more to the BET surface area of Rh/Z, so that the contacts created in mechanical mixtures are mostly between Rh/A and Rh supported on tetragonal zirconia. Then, the cooperative effect in the catalytic activity would mainly involve Rh supported on tetragonal zirconia, and it can be admitted that the monoclinic phase does not significantly influence catalytic performance, even though is present in bulk zirconia.

Furthermore, it has been reported in literature [45] that Rh supported on tetragonal zirconia is much more active for the dissociative adsorption of C—H than Rh supported on monoclinic zirconia. Then, we can admit that Rh supported on tetragonal zirconia is the main active phase in the grafted ZrO_2 and also in the bulk ZrO_2. This means that the improved activity of Rh/100Z-A, compared to an equivalent mixture of Rh/A and Rh/Z, cannot be

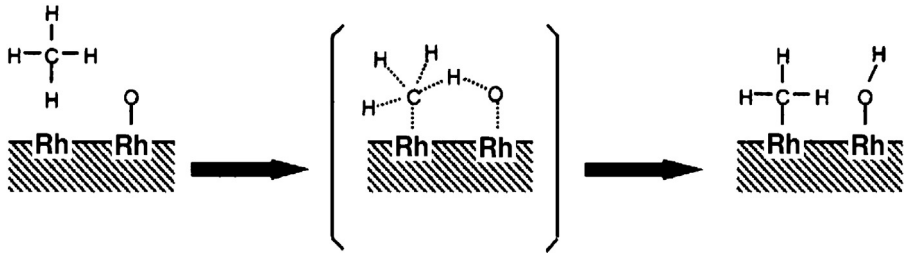

Scheme 3. Oxygen-assisted dissociation pathway for methane activation [42,43].

attributed to the structural differences between grafted and bulk zirconia.

In conclusion, it can be suggested that the synergy occurring in the mixtures is magnified in the grafted catalyst, which contains a larger number of contact points between the alumina support and the ZrO_2 crystallites formed on its surface. It can be noted that an optimization of the grafting process of Zr on the alumina surface might lead to a further improvement of the activity.

5. Conclusions

This work deals with the understanding of the dynamic processes occurring in Rh supported catalysts during dry reforming of methane, and their implications in the catalytic activity.

γ-Al_2O_3 was modified by grafting a small amount of zirconia on its surface. Then Rh was deposited following the same procedure as for the non-modified supports. A significant improvement of the catalytic performance was obtained with the grafted catalyst, which is apparently formed by Rh/γ-Al_2O_3 and Rh/ZrO_2 particles in physical contact. To further understand this high activity, mechanical mixtures of separately prepared Rh/γ-Al_2O_3 and Rh/ZrO_2 catalysts were synthesized. Rh/ZrO_2 single catalyst presents a very low activity, while Rh/γ-Al_2O_3 presents a high activity. A completely reduced Rh surface does not seem to be optimal for DRM, which is better conducted over a surface where well-dispersed metallic Rh sites coexist along with a high amount of oxidized sites. Compared with single catalysts, the mixtures with low content of Rh/ZrO_2 exhibit a higher activity and an important synergistic effect is observed. The synergistic effect observed in the mechanical mixtures, would occur mainly through the physical contact between Rh/γ-Al_2O_3 and Rh/ZrO_2, as separated catalytic phases. Then, a catalytic cooperation is also expected between the Rh/γ-Al_2O_3 and Rh/ZrO_2 particles present in the grafted catalyst. A possible explanation of this effect is the modulation of the Rh oxidation state on Rh/ZrO_2 by the Rh/γ-Al_2O_3 catalyst. At reaction conditions, the oxygen species, originated from the dissociative adsorption of CO_2 over Rh/γ-Al_2O_3, could migrate to Rh/ZrO_2 promoting the oxidation of rhodium in it. It is suggested that the cooperative effect is magnified in the grafted sample, which presents a high quality and number of contacts between Rh/γ-Al_2O_3 and Rh/ZrO_2, thus explaining its high activity. The presence of metallic and oxidized Rh seems to be a crucial parameter for high catalytic performance in DRM.

Acknowledgements

The authors are grateful to the Chilean Government for supporting this study, through PFB 27/CCTE-UDT and FONDECYT 1101005 grants. The authors gratefully acknowledge the "Direction Générale des Technologies, de la Recherche et de l'Energie (DGTRE)" of the "Région Wallonne" (Belgium) and the "Fonds National de la Recherche Scientifique (FNRS)" of Belgium, for their financial support. The involvement of Unité de catalyse et de chimie des matériaux divisés (IMCN, MOST) in the «INANOMAT» IUAP network sustained by the «Service public fédéral de Programmation Politique Scientifique» (Belgium) is acknowledged.

References

[1] M. Gadalla, B. Bower, Chem. Eng. Sci. 43 (1988) 3049–3062.
[2] I. Wender, Fuel Process. Technol. 48 (1996) 189–297.
[3] J. Wei, E. Iglesia, J. Catal. 225 (2004) 116–127.
[4] Z.P. Liu, P. Hu, J. Am. Chem. Soc. 125 (2003) 1958–1967.
[5] S.B. Wang, G.Q.M. Lu, G.J. Millar, Energy Fuels 10 (1996) 896–904.
[6] A. Erdöhelyi, J. Cserényi, F. Solymosi, J. Catal. 141 (1996) 287–299.
[7] J.R. Rostrup-Nielsen, J.H.B. Hansen, J. Catal. 144 (1993) 38–49.
[8] J.H. Bitter, K. Seshan, J.A. Lercher, J. Catal. 176 (1998) 93–101.
[9] P. Ferreira-Aparicio, A. Guerrero-Ruiz, I. Rodríguez-Ramos, Appl. Catal. A 170 (1998) 177–187.
[10] P. Ferreira-Aparicio, M. Fernández-García, A. Guerrero-Ruiz, I. Rodríguez-Ramos, J. Catal. 190 (2000) 296–308.
[11] M.F. Mark, W.F. Maier, J. Catal. 164 (1996) 122–130.
[12] M.F. Mark, F. Mark, W.F. Maier, Chem. Eng. Technol. 20 (1997) 361–370.
[13] M. Nagai, K. Nakahira, Y. Ozawa, Y. Namiki, Y. Suzuki, Chem. Eng. Sci. 62 (2007) 4998–5000.
[14] U.L. Portugal, A. Santos, S. Damyanova, C.M.P. Marques, J.M.C. Bueno, J. Mol. Catal. A: Chem. 184 (2002) 311–322.
[15] R.W. Stevens, S.S.C. Chuang, J. Phys. Chem. B 108 (2004) 696–703.
[16] H.Y. Wang, E. Ruckenstein, Appl. Catal. A 204 (2000) 143–152.
[17] Z.L. Zhang, V.A. Tsipouriari, A.M. Efstathiou, X.E. Verykios, J. Catal. 158 (1996) 51–63.
[18] P. Hwang, C.T. Yeh, Q. Zhu, Catal. Today 51 (1999) 93–101.
[19] R. Burch, P.K. Loader, Appl. Catal. A 143 (1996) 317–335.
[20] H. Li, J. Wang, Chem. Eng. Sci. 59 (2004) 4861–4867.
[21] S. Therdthianwong, A. Therdthianwong, C. Siangchin, S. Yongprapat, Int. J. Hydrogen Energy 33 (2008) 991–999.
[22] M.M.V.M. Souza, D.A.G. Aranda, M. Schmal, J. Catal. 204 (2001) 498–511.
[23] P. Iengo, M. Di Serio, V. Solinas, D. Gazzoli, G. Salvio, E. Santacesaria, App. Catal. A 170 (1998) 225–244.
[24] C. Mateos-Pedrero, S.R.G. Carrazán, P. Ruiz, Catal. Today 112 (2006) 107–111.
[25] R. Monaci, E. Rombi, V. Solinas, A. Sorrentino, E. Santacesaria, G. Colon, Appl. Catal. A 214 (2001) 203–212.
[26] J.D. McCullough, K.N. Trueblood, Acta Crystallogr. 12 (1959) 507–511.
[27] Aspen HYSYS 2006; software for chemical process simulation, Aspen Technology Inc., 2006.
[28] F.P.J.M. Kerkhof, J.A. Moulijn, J. Phys. Chem. 83 (1979) 1612–1619.
[29] N.G. Peela, A. Mubayi, D. Kunzru, Chem. Eng. J. 167 (2011) 578–587.
[30] H.W. Jen, G.W. Graham, W. Chun, R.W. McCabe, J.P. Cuif, S.E. Deutsch, O. Touret, Catal. Today 50 (1999) 309–328.
[31] M.C.J. Bradford, M.A. Vannice, Appl. Catal. A 142 (1996) 97–122.
[32] S. Damyanova, P. Grange, B. Delmon, J. Catal. 168 (1997) 421–430.
[33] Z. Weng-Sieh, R. Gronsky, A.T. Bell, J. Catal. 170 (1997) 62–74.
[34] K. Doi, Y.Y. Wu, R. Takeda, A. Matsunami, N. Arai, T. Tagawa, S. Goto, Appl. Catal. B 35 (2001) 43–51.
[35] M. Ojeda, S. Rojas, F.J. Garcia-Garcia, M.L. Granados, P. Terreros, J.L.G. Fierro, Catal. Commun. 5 (2004) 703–707.
[36] A. Guerrero-Ruiz, I. Rodriguez-Ramos, Spillover and Mobility of Species on Solid Surfaces, vol. 138, 1st ed., Elsevier Science B.V., Madrid, 2001.
[37] W.C. Conner Jr., J.L. Falconer, Chem. Rev. 95 (1995) 708–759.
[38] A. Beuls, C. Swalus, M. Jacquemin, G. Heyen, A. Karelovic, P. Ruiz, Appl. Catal. 113–114 (2012) 2–10.
[39] M. Jacquemin, A. Beuls, P. Ruiz, Catal. Today 157 (2010) 462–466.
[40] F. Dury, E.M. Gaigneaux, P. Ruiz, Appl. Catal. A 242 (2003) 187–303.
[41] A.N.J. Van Keulen, K. Seshan, J.H.B.J. Hoebink, J.R.H. Ross, J. Catal. 166 (1997) 306–314.
[42] C.T. Au, M.S. Liao, C.F. Ng, Chem. Phys. Lett. 267 (1997) 44–50.
[43] K. Fujimoto, F.H. Ribeiro, M. Avalos-Borja, E. Iglesia, J. Catal. 179 (1998) 431–442.
[44] A. Yamaguchi, E. Iglesia, J. Catal. 274 (2010) 52–63.
[45] M.C. Campa, G. Ferraris, D. Gazzoli, I. Pettiti, D. Pietrogiacomi, Appl. Catal. B 142 (2013) 423–431.